Desalination and Water Treatment
www.deswater.com
doi: 10.5004/dwt.2020.25040

179 (2020) 197–210
March

Simultaneous adsorption of Cr(VI) and fluoride from aqueous over multiple-metal layer double hydroxides: performance and mechanism

He Wang, Wei Liao, Hui-qiang Li*

College of Architecture and Environment, Sichuan University, Chengdu 610065, China, Tel. +8618011446490, +8618200288011, +8618980668020; emails: lhq_scu@163.com (H.-q. Li), wh_820@163.com (H. Wang), Lwei0314@163.com (W. Liao)

Received 7 May 2019; Accepted 12 October 2019

ABSTRACT

A series of multiple-metal layer double hydroxides: MgAl-LDH, CoMgAl-LDH and CoZnMgAl-LDH were prepared for single/simultaneous adsorption of Cr(VI) and fluoride from aqueous solution. X-ray powder diffraction, Fourier transform infrared spectroscopy, Brunauer–Emmett–Teller, scanning electron microscope and energy-dispersive X-ray analyses techniques were employed to characterize the as-prepared LDHs. The CoMgAl-LDH displayed the best Cr(VI) and fluoride adsorption performance compared with the other LDHs. In single pollutant removal system, the maximum adsorption capacities of 52.63 and 29.41 mg/g for Cr(VI) and fluoride were calculated from the Langmuir isotherm with an initial pH value of 7. Competitive adsorption between Cr(VI) and fluoride was observed during simultaneous adsorption, and the affinity of Cr(VI) on the LDHs was stronger than that of fluoride. The presence of Co was found to be responsible for the enhanced defluorination of CoMgAl-LDH. The pseudo-second order equation and the Langmuir adsorption isotherm fitted well to the adsorption data of Cr(VI) and fluoride. Ion exchange was the main way to remove Cr(VI) and fluoride by LDHs.

Keywords: Multiple metal; Layer double hydroxides; Cr(VI); Fluoride; Simultaneous adsorption

1. Introduction

Cr(VI) and fluoride produce harmful effect on environmental system. Chromium in the environment mainly exists in two forms (Cr(III) and Cr(VI)), and Cr(VI) is highly toxic, carcinogenic and teratogenic [1]. Main anthropogenic activity and accidental natural geogenic activity are responsible for Cr(VI) release into the environment. According to literature, Mediterranean (Greece, Italy and Pacific [California {USA}], Mexico) and different parts of the world are the few populated areas, which are the examples of such conditions [2]. Fluoride appears in groundwater around the world. Other than industrial production, the natural geological sources such as fluorine-containing rocks also account for the fluoride release [3]. The maximum concentration limit for Cr(VI) and fluoride is 0.05 and 1.5 mg/L, respectively, according to World Health Organization (WHO) guidelines for drinking water quality [4].

In previous literatures, various methods have been applied to remove anionic contaminants from aqueous solution, including adsorption [5], photoremediation [6], ion exchange [7], etc. Among the various methods discussed for the removal of different contaminants, adsorption has been used successfully because of its remarkable easy operation, high efficiency, low cost and without secondary pollution [8]. The adsorbents developed for purification of aqueous solutions include carbon [9], nanocomposite hydrogels [10], and agricultural waste [11], etc. Known as a natural clay with good environment compatibility, high anion exchange ability and easy synthesis, layered double hydroxides (LDHs) are

* Corresponding author.

1944-3994/1944-3986 © 2020 Desalination Publications. All rights reserved.

considered to be efficient adsorbents for anionic contaminants removal from aqueous solution, such as F^- [12] and $Cr_2O_7^{2-}$ [13].

Recently, numerous researchers have focused on modification of LDHs to improve the physical/chemical properties by applying various materials such as polyoxometalate [14], heptamolybdate [15], nanocomposite [7], etc. Some novel synthetic methods are also employed, such as exfoliated LDH nanosheets [16]. However, accepted formula of LDHs is $[M^{II}_{1-x}M^{III}_x(OH)_2](A^{n-})_{x/n}\cdot mH_2O$, where M^{II} represents divalent metal ion (Ca^{2+}, Mg^{2+}, Zn^{2+}, Co^{2+}, etc.) and M^{III} represents trivalent metal ion (Al^{3+}, Fe^{3+}, Cr^{3+}, etc.) [17]. Innate property of the LDHs is generally determined by the metal composition [18]. As the main components, M^{II} and M^{III} can be replaced by different metal ions, so that LDHs with different characters can be prepared by replacing M^{II} and M^{III} species [19]. Cai et al. [20] find ternary LiAlLa-LDH has an enhanced capacity than binary LiAl-LDH for fluoride removal after the introduction of La. Fe(II)Al-LDH prepared by He et al. [21] can transform Cr(VI) into Cr(III) to remove Cr(VI) utilizing the strong reductive property of Fe(II). Here we introduce Co^{2+} and Zn^{2+} into M^{II} components of the LDHs to prepare MgAl-LDH, CoMgAl-LDH and CoZnMgAl-LDH via co-precipitate method to remove Cr(VI) and fluoride in the single/simultaneous system.

To the best of our knowledge, the performance and mechanism of single/simultaneous adsorption of Cr(VI) and fluoride has not been reported yet, especially using a series of multiple-metal LDHs. The main objectives were: (1) comparing the removal efficiency and adsorption capacity between single Cr(VI) or fluoride and simultaneous Cr(VI)-fluoride system; (2) studying the structure and property of the LDHs before and after adsorption, (3) figuring out the adsorption mechanism of Cr(VI) and fluoride by the LDHs.

2. Materials and methods

2.1. Reagents

All reagents used in this study were analytical grade (purity ≥ 99.7%) without further purification. Aluminum chloride [$AlCl_3\cdot6H_2O$], magnesium chloride [$MgCl_2\cdot6H_2O$], zinc chloride [$ZnCl_2\cdot6H_2O$], cobalt chloride [$CoCl_2\cdot6H_2O$], sodium hydroxide [NaOH], hydrochloric acid [HCl], sodium fluoride [NaF] and potassium bichromate [$K_2Cr_2O_7$] were obtained from Sigma-Aldrich (Shanghai, China).

2.2. Preparation of the LDHs

A series of LDHs: MgAl-LDH, CoMgAl-LDH and CoZnMgAl-LDH were prepared by the co-precipitation method as described elsewhere [22]. Analytical grade $MgCl_2\cdot6H_2O$ (0.06 M) and $AlCl_3\cdot6H_2O$ (0.02 M) were dissolved in deionized water. Another solution containing analytical grade NaOH (2.0 M) and NaCl (1.0 M) in deionized water was prepared. The two solutions were simultaneously added to one flask under vigorous stirring (700 rpm) and stirred for 60 min. During the synthesis procedure, pH of the solution was kept around 10 using 2.0 mol NaOH and stirred for 120 min at room temperature. After that, the mixture was aged in the mother liquor at 80°C for 24 h. Then, the products were centrifuged and washed thoroughly with deionized water until pH of the wash solution was neutral. Finally, the washed samples were then dried at 65°C for 24 h to obtain MgAl-LDH. Similarly, CoMgAl-LDH and CoZnMgAl-LDH were obtained as described above. In detail, $CoCl_2\cdot6H_2O$ (0.02 M), $MgCl_2\cdot6H_2O$ (0.04 M) and $AlCl_3\cdot6H_2O$ (0.02 M) were prepared to obtain the CoMgAl-LDH. CoZnMgAl-LDH was obtained by adding $CoCl_2\cdot6H_2O$ (0.02 M), $MgCl_2\cdot6H_2O$ (0.02 M), $AlCl_3\cdot6H_2O$ (0.02 M) and $ZnCl_2\cdot6H_2O$ (0.02 M) into the salt solution.

2.3. Characterization of the LDHs

Crystalline structure of the LDHs was determined by X-ray powder diffraction (XRD) employing a scanning rate 4°/min over an angular range 2θ between 10° and 80° with Cu Kα as source of radiation (PANalytical B.V., Holland). The specific surface areas were achieved by N_2 adsorption based on Brunauer–Emmett–Teller (BET) method at –196°C with an ASAP 2020 apparatus. The surface area and total pore volume were calculated according to the BET model while the pore size distribution was determined by the non-local density functional theory method with a slit pore model. Analysis of Fourier transform infrared spectroscopy (FTIR) spectra enabled evaluation of surface functionality of the LDHs, and their variations after adsorption of Cr(VI) and fluoride. The spectra were obtained in the attenuated total reflection mode ranging from 0 to 4,000 cm^{-1} with a 2 cm^{-1} resolution (Nicolet 6700, USA). Scanning electron microscope (SEM) images and energy-dispersive X-ray analyses (EDX) analyses were taken on a Hitachi S4800 field-emission scanning electron microscope.

2.4. Adsorption experiments

Batch experiments were performed to investigate adsorption performance of Cr(VI) and fluoride on the LDHs. The stock solution was prepared by dissolving potassium dichromate and sodium fluoride in deionized water, respectively. The pH was adjusted to about 7 with 0.1 M HCl or NaOH. All batch studies were carried out by mixing adsorbents with 50 mL of the solution containing 10 mg/L of Cr(VI) or fluoride in a thermostatic shaker at 298 K and 500 rpm. The dosage of LDHs was changed at 0.2, 0.5, 0.7 and 1.0 g/L, respectively. The samples were filtered with 0.45 μm filter to obtain the concentrations of Cr(VI) and fluoride. Analysis of Cr(VI) was achieved by 1,5-diphenylcarbohydrazide method [1]. Fluoride concentration was measured by a fluoride ion selective electrode (PF-1) with sodium citrate ($C_6H_5Na_3O_7$, 0.2 mol/L) and $NaNO_3$ (1 mol/L) as total ion strength adjustment buffer [23]. Simultaneous adsorption was investigated by adding adsorbents to the mixed solution that contains Cr(VI) and fluoride with 10 mg/L each.

The adsorption capacity (q_t) and removal percentage (R%) of the adsorbents are calculated according to the following equations [24]:

$$q_t = \frac{(C_0 - C_t)V}{m} \tag{1}$$

$$R\% = \frac{(C_0 - C_t)}{C_0} \times 100\% \tag{2}$$

where C_0 and C_t (mg/L) are the liquid-phase concentrations of Cr(VI) or fluoride at initial and at time t, respectively. V is the volume (mL) of solution, and m (mg) is the mass of adsorbent used.

3. Results and discussion

3.1. Characterization of the LDHs

The XRD patterns of the LDHs are shown in Fig. 1a. Diffraction peaks were observed at 11.16° (003), 22.56° (006), 34.45° (012), 38.51° (015), 60.26° (110) and 61.45° (113) for all samples which exhibited the characteristic diffractions of well-crystallized hydrotalcite-like LDHs [25]. The peaks were sharp and symmetric, which are sufficient to prove that high-purity LDHs were synthesized [26]. In addition, the diffraction peaks of CoMgAl-LDH and CoZnMgAl-LDH located at 31.72° could be assigned to $Co_6Al_2O_{11}$ (JCPDS card No.51-0041). The excess diffraction peaks of CoZnMgAl-LDHs observed at 56.49°, 65.17° and 75.3° could be assigned to $Zn(OH)_2$ (JCPDS card No.41-1359), $Al_{13}Co_4$ (JCPDS card No.50-0694) and $AlMg_4Zn_{11}$ (JCPDS card No.31-0024). The d_{003} values of MgAl-LDH, CoMgAl-LDH and CoZnMgAl-LDH were 0.782, 0.792 and 0.802 nm, respectively, corresponding to the basal spacing of two coherent brucite-like hydroxide layers in the LDHs [27]. The expanded values of d_{003} indicated the successful introduction of Co and Zn into the LDHs structure. The observed lattice parameter d_{003} of the LDHs was similar to other LDHs reported elsewhere [28].

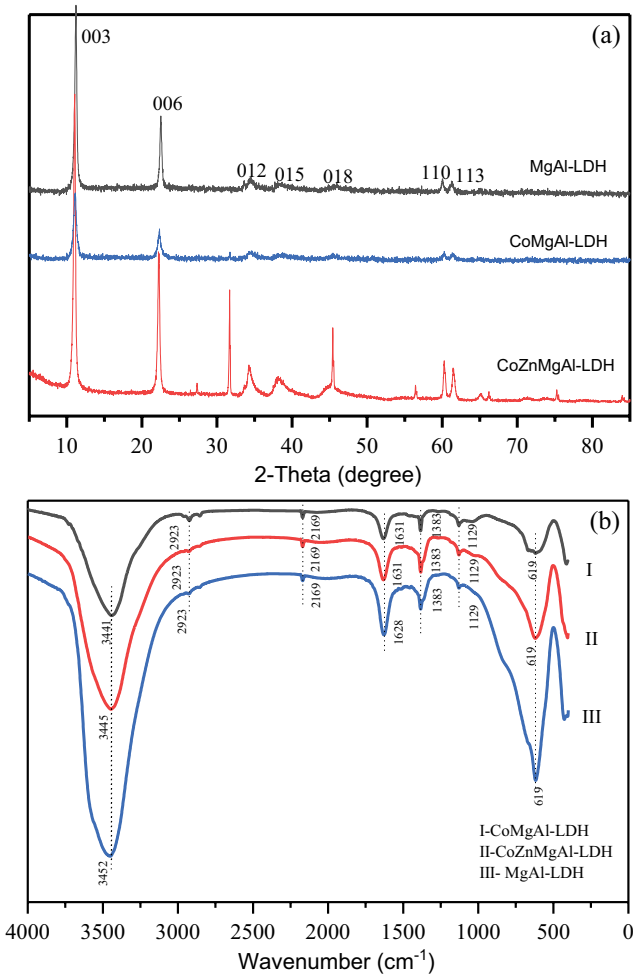

Fig. 1. (a) XRD patterns for the LDHs and (b) FTIR spectra for the LDHs from 0 to 4,000 cm^{-1}.

The surface functional groups were recognized as a critical factor that determined the adsorption behavior [29]. FTIR spectra for different samples were carried out in the range of 0–4,000 cm^{-1}. The LDHs exhibit a similar FTIR spectrum in Fig. 1b. The main band in MgAl-LDH was 3,452 cm^{-1} which could be assigned to the stretching vibration of O–H groups [30]. It shifted to lower wavelength in CoZnMgAl-LDH (3,445 cm^{-1}) and CoMgAl-LDH (3,441 cm^{-1}). The changes may be accounted for the increased hydrogen bonding between the surface and interlayer [28]. Additionally, the shoulder band around 2,923 cm^{-1} could be assigned to hydrogen bonding between hydroxyl/water molecules and carbonate anions [15]. The peak at 1,630 cm^{-1} was related to the O–H stretching of water molecules, being adsorbed or present in the interlayer region [14]. The peaks around 2,169 and 1,383 cm^{-1} were contributed to the stretching vibration of CO_3^{2-}, indicating a handful of CO_2 entered into the interlayers during the synthesis of the LDHs. The lowered region (below 1,000 cm^{-1}) was significant, and a strong adsorption band was observed at 619 cm^{-1} in all LDHs spectra, which can be attributed to the M–O and M–O–M lattice vibration [28]. The FTIR spectra revealed that all the LDHs contained abundant oxygen functional groups, which served as available adsorption sites and further discussion would be provided later.

The N_2 adsorption–desorption isotherms and the pore size distribution calculated with Barrett–Joyner–Halenda method are shown in Fig. 2. Adsorption isotherms of the LDHs were similar, and the adsorption and desorption curves contained H3-type hysteresis loops [31], which conformed to a type-IV adsorption isotherm according the IUPAC classification. The results indicated that the three LDHs were all mesoporous materials [26]. In addition, the average pore size of the LDHs samples also showed mesopore size (2–50 nm) in the adsorbents, which endowed large specific surface area. The surface area followed the order: CoMgAl-LDH (48.0 m^2/g) > MgAl-LDH (40.7 m^2/g) > CoZnMgAl-LDH (30.6 m^2/g). CoMgAl-LDH exhibited the highest surface area after being loaded with Co and CoZnMgAl-LDH showed the smallest surface area due to the distortion of crystals resulting from Zn insertion into the lattice. Compared with the similar LDHs reported in previous studies [15], the BET surface area and pore volume of the CoMgAl-LDH were similar with them.

3.2. Single/simultaneous adsorption

3.2.1. Adsorption behavior of Cr(VI)

Effect of adsorbent dose on Cr(VI) removal is shown in Fig. 3. At a dose of 0.2 g/L (Fig. 3a), the removal efficiency on the LDHs was obviously enhanced with time. It was attributed to the availability of more active sites on the adsorbents. At a dose of 0.5 g/L (Fig. 3b), the adsorption on the LDHs was more rapid and the maximum removal rate occurred

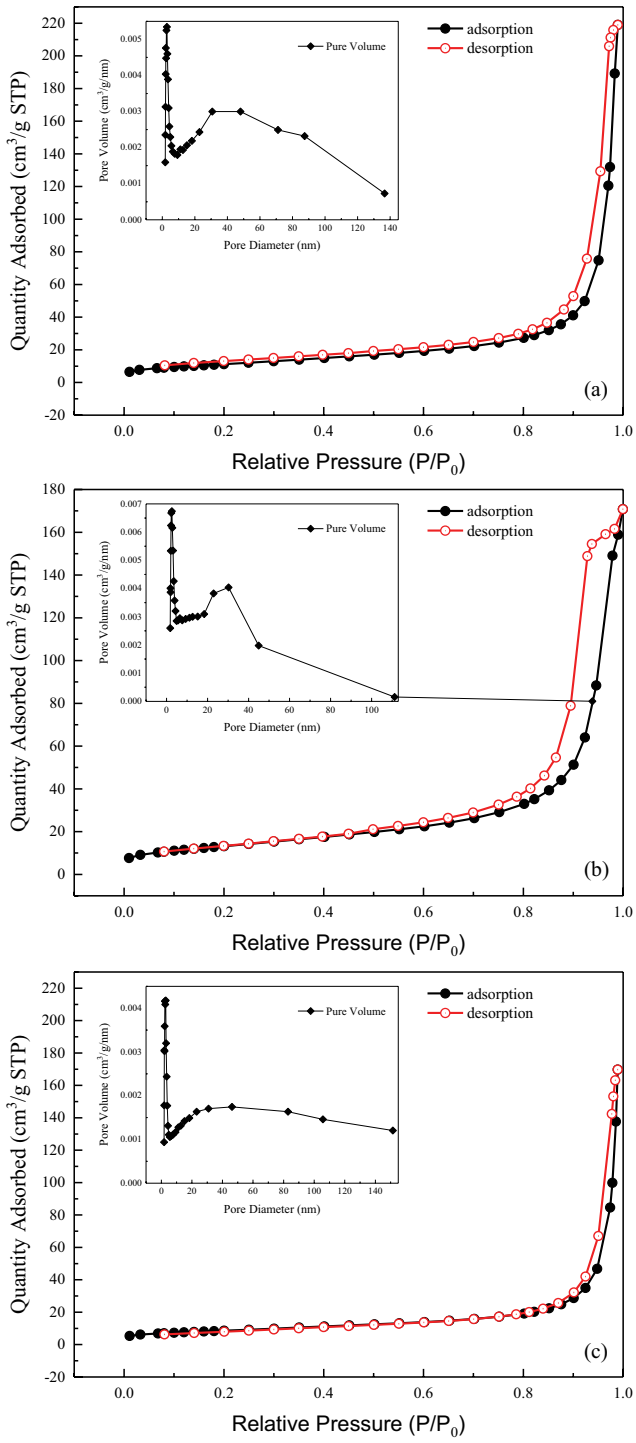

Fig. 2. Isotherm curve of N_2 adsorption–desorption and pore size distribution of (a) MgAl-LDH, (b) CoMgAl-LDH and (c) CoZnMgAl-LDH.

at the first 30 min. CoMgAl-LDH achieved the removal rate more than 99.5%. Although the removal rate on CoZnMgAl-LDH was similar with CoMgAl-LDH, a slight desorption occurred on CoZnMgAl-LDH. By contrast, removal rate on MgAl-LDH was only 93% and instable. As the adsorbent dose rose to 0.7 g/L (Fig. 3c), the phenomenon of desorption faded away. Saturation adsorption was achieved and there was no evident promotion in Cr(VI) removal with the dose rose further to 1.0 g/L (Fig. 3d). The result would be caused by the overlapping of active sites at a higher adsorbent dose [32]. At a suitable adsorbent dose, entire surface sites were available for the target pollutant and surplus active sites on redundant adsorbent would eliminate desorption. When the adsorbent was excessive, particle aggregation was created by collision among solid particles probably, resulted in a decrease in the total surface area and active sites [33]. In all cases, CoMgAl-LDH showed the superior performance than the other LDHs.

3.2.2. Adsorption behavior of fluoride

As to fluoride, the weakly ionized hydrogen fluoride (HF) formed when pH was below 4, and the pH higher than 10 would lead to the dissolution of aluminum from the layered structure. In order to eliminate the interference of pH on adsorption performance, the initial pH value of the stock solution was adjusted to around 7 which belonged to the effective initial pH for fluoride removal. Removal efficiencies of fluoride on different doses are shown in Fig. 4. The adsorption capacity slowly increased with contact time and tended to saturation at 50 min. Noteworthy, no desorption of fluoride on the LDHs was observed in all cases. The result could be attributed to that chloride ions exchanged by fluoride in solution have little effect on fluoride removal as previously reported [31]. With 0.2 g/L dosage (Fig. 4a), only 47.5% fluoride was removed, suggesting insufficient dosage is a constraint factor under this situation [34]. The removal rate improved with the adsorbent dose increased from 0.2 to 1.0 g/L, and the removal capacity of the CoMgAl-LDH expanded slowly and gradually stabilized with maximum removal efficiency of about 90%. CoMgAl-LDH showed the most effective fluoride removal efficiency than MgAl-LDH and CoZnMgAl-LDH. The promotion of CoMgAl-LDH might be ascribed to the composition of Co. After doping Co into the MgAl-LDH, the removal rate showed distinct improvement from 78% to 90%. Besides Co, according to the previous report, doping the metal La or Ce into the framework of LDHs could also improve the adsorption performance [35,36]. In addition, the suitable structure of the CoMgAl-LDH with a larger BET area and a favorable pore distribution would be in favor of the adsorption as well.

3.2.3. Simultaneous adsorption

In groundwater, co-existing anions would interfere with each other. Fluoride ions and Cr(VI) competed for the adsorption sites and pollutant adsorption capacity would be affected [37]. The simultaneous adsorption experiments on Cr(VI) and fluoride removal were conducted in a mixed solution containing 10 mg/L of Cr(VI) and fluoride each. The results are shown in Figs. 5 and 6. Obviously, in simultaneous adsorption, the removal capacities of Cr(VI) and fluoride on the LDHs were lower than those in the single adsorption due to the presence of competitive adsorption. In simultaneous adsorption, CoMgAl-LDH showed better performance than the other LDHs.

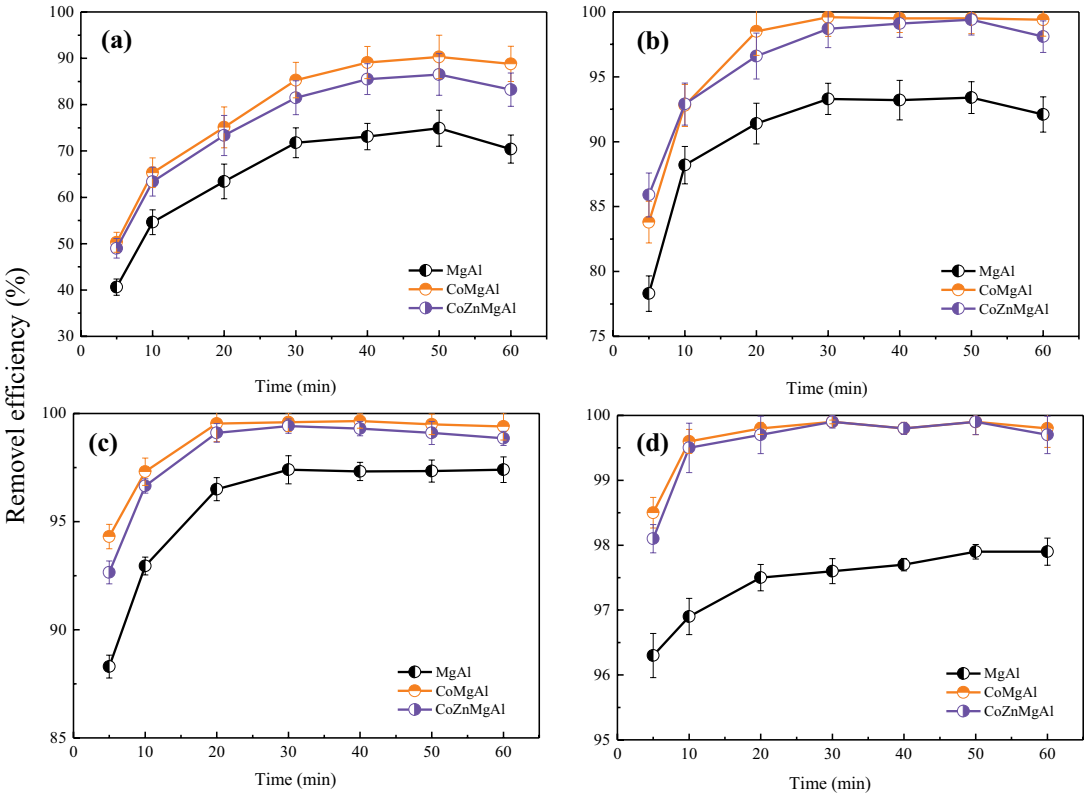

Fig. 3. Different dosages of the LDHs for Cr(VI) removal at initial pH about 7, 10 mg/L and 298 K. (a) 0.2, (b) 0.5, (c) 0.7 and (d) 1.0 g/L.

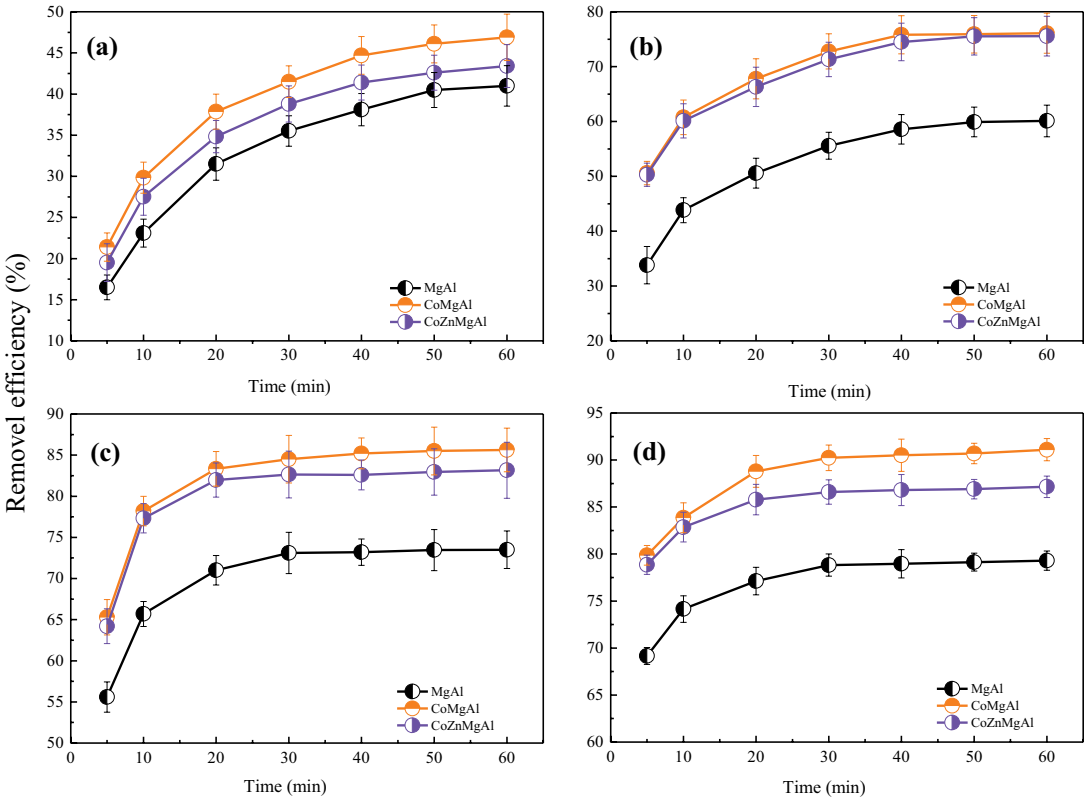

Fig. 4. Different dosages of the LDHs for fluoride removal, at initial pH about 7, 10 mg/L and 298 K. (a) 0.2, (b) 0.5, (c) 0.7 and (d) 1.0 g/L.

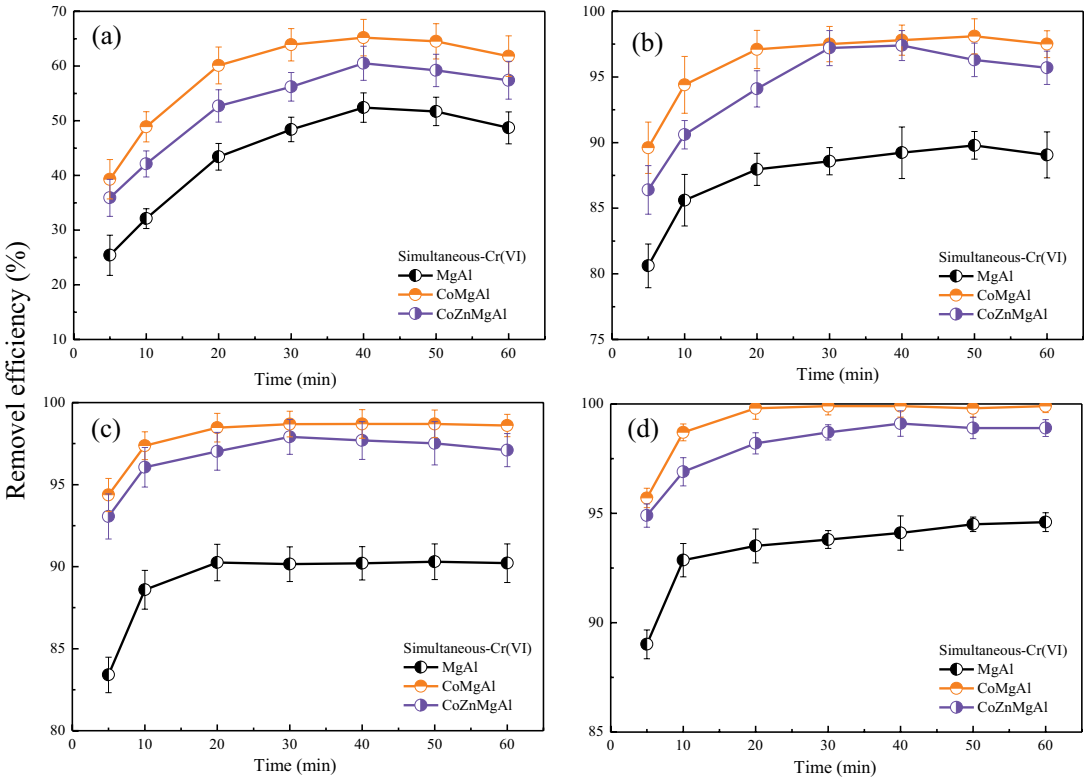

Fig. 5. Removal rate of Cr(VI) in simultaneous adsorption (initial concentration of F^- and Cr(VI) is 10 mg/L, respectively, T = 298 K, initial pH about 7, adsorbent dosage: (a) 0.2, (b) 0.5, (c) 0.7 and (d) 1.0 g/L.

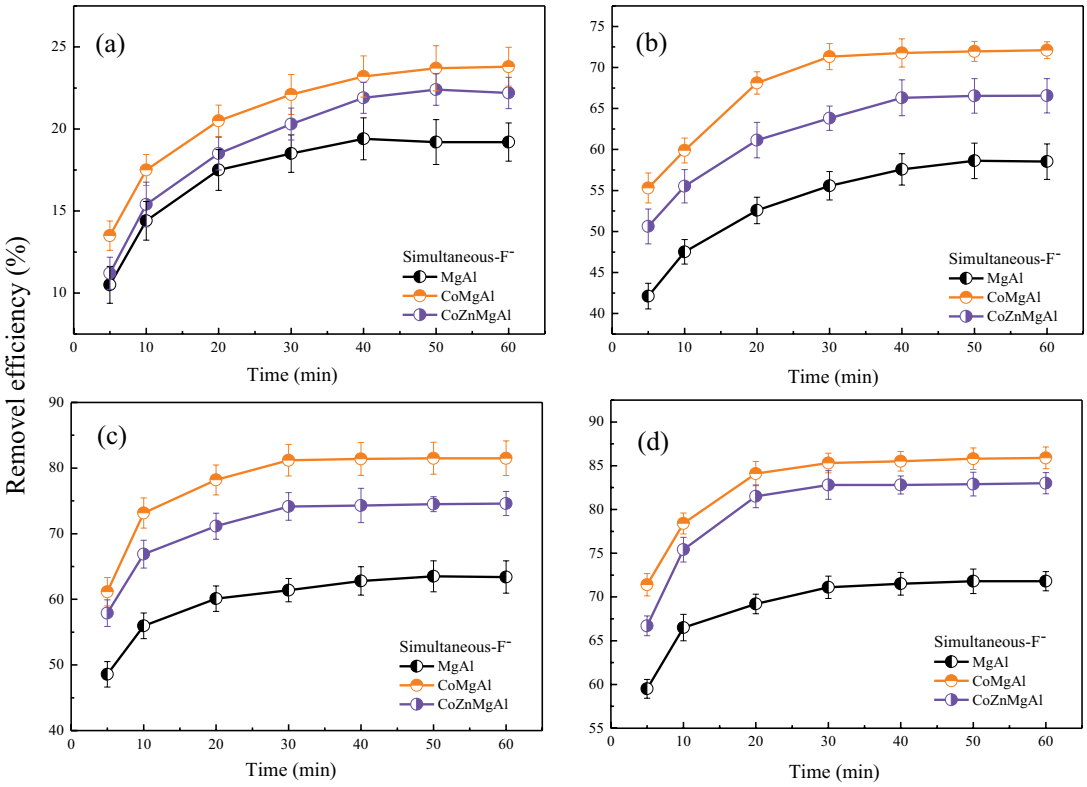

Fig. 6. Removal rate of F^- in simultaneous adsorption (initial concentration of F^- and Cr(VI) is 10 mg/L, respectively, T = 298 K, initial pH about 7, adsorbent dosage: ((a) 0.2, (b) 0.5, (c) 0.7 and (d) 1.0 g/L).

The removal rate of Cr(VI) in simultaneous adsorption increased slower than in single adsorption with time and the maximum adsorption appeared after 40 min. With further increasing contact time from 40 to 60 min, a conspicuous desorption was observed (Fig. 5a). Similar phenomenon appeared in other reports. Ling et al. [25] reported that desorption phenomenon occurred at 10 mg/L of Cr(VI) by CoFe-LDH. Desorption of Cr(VI) ions from adsorbed LDHs was dependent upon the nature of anions present in the solution. The amount of Cr(VI) that was replaced from LDHs by competing anions followed the order CO_3^{2-} > Cl^- > water [38], which reflected the relative affinity of anions for the LDHs. At the beginning of adsorption, the overwhelming majority of Cr(VI) accessed into interlayer of the LDHs by ion exchange with Cl^-. When the adsorption process approached equilibrium, the Cr(VI) adsorbed in the interlayer edge of the LDHs would be replaced by the excessive Cl^-. However, to increase the dose of adsorbent would eliminate the desorption of Cr(VI), by providing additional active sites for adsorption according to Fig. 5.

In single adsorption of Cr(VI), the maximum removal capacity calculated by the Langmuir model was 52.63 mg/g which is shown in Table 2. The value reduced to 38.3 mg/g in the simultaneous adsorption of Cr(VI) that was equal about 24% weakened by co-existing fluoride. On the other hand, there was a significant decrease of defluorination capacity from 29.41 to 13.74 mg/g that was equal about 53% weakened by co-existing Cr(VI). The results indicated that Cr(VI) adsorbed by the LDHs was much stronger than fluoride. The weakening effect could be ascribed to two reasonable explanations: (1) Cr(VI) had more powerful affinity than fluoride to the LDHs in simultaneous adsorption. When faced with the two ions in one solution, Cr(VI) would occupy the active sites preferentially resulting in a decrease in the total available active sites and make the adsorption of fluoride more weak; (2) part of surface mesoporous of the LDHs might be covered or blocked by the adsorbed Cr(VI) and eventually resulted in a decreased amount of contact area for fluoride adsorption.

According to the above results of experiments and characterizations, CoMgAl-LDH showed superior adsorption performance than MgAl-LDH and CoZnMgAl-LDH due to the better degree of crystallinity, higher BET surface area and abundant hydroxyl groups.

3.2.4. Kinetics and isotherms study

Kinetic models help in evaluating the rate of adsorption and the type of reaction mechanism involved. Therefore, linear pseudo-first order and pseudo-second order kinetic models were applied to fit the experimental data and the equations are represented as follows [39]:

Pseudo-first order:

$$\log\left(q_e - q_t\right) = \log q_e - \frac{k_1}{2.303}t \tag{3}$$

Pseudo-second order:

$$\frac{t}{q_t} = \frac{1}{k_2 q_e^2} + \frac{1}{q_e}t \tag{4}$$

where q_t (mg/g) and q_e (mg/g) are adsorption amounts of the adsorbents at time t and at equilibrium, respectively. The values of rate constant k_1 (min^{-1}) and k_2 [g/mg/min] are determined from the slopes of the plots $\log(q_e–q_t)$ vs. t and t/q_t vs. time, respectively. The values of different constants and correlation coefficients from the fitted kinetic models are presented in Table 1. It was found that the value of correlation coefficients (R^2) for pseudo-second order was higher than that of pseudo-first order whether it was in single adsorption or simultaneous adsorption. The results implied that Cr(VI) and fluoride adsorption was a process described perfectly by pseudo-second order models (Fig. 7). The results indicated that the adsorption of Cr(VI) and fluoride onto LDHs surface occurred via chemical interactions [9].

Table 1
Kinetic parameters for the single/simultaneous adsorption of Cr(VI) and fluoride on the LDHs with dosage at 0.7 g/L

Item		Pseudo-first order			Pseudo-second order		
		K_1 (min^{-1})	q_e (mg/g)	R^2	K_2 (g/mg/min)	q_e (mg/g)	R^2
Single-Cr(VI)	MgAl-LDH	0.094	34.64	0.993	0.023	40.43	0.998
	CoMgAl-LDH	0.098	42.92	0.984	0.004	49.06	0.999
	CoZnMgAl-LDH	0.100	39.97	0.958	0.005	46.65	0.999
Single-F^-	MgAl-LDH	0.070	20.92	0.977	0.004	23.44	0.999
	CoMgAl-LDH	0.082	22.75	0.959	0.005	26.00	0.999
	CoZnMgAl-LDH	0.075	21.70	0.976	0.005	24.19	0.999
Simultaneous-Cr(VI)	MgAl-LDH	0.076	26.17	0.996	0.005	29.34	0.996
	CoMgAl-LDH	0.080	32.20	0.994	0.008	35.11	0.999
	CoZnMgAl-LDH	0.080	29.86	0.997	0.007	32.27	0.999
Simultaneous-F^-	MgAl-LDH	0.051	9.46	0.978	0.020	10.50	0.997
	CoMgAl-LDH	0.060	12.89	0.970	0.017	12.65	0.997
	CoZnMgAl-LDH	0.056	11.13	0.997	0.013	12.22	0.990

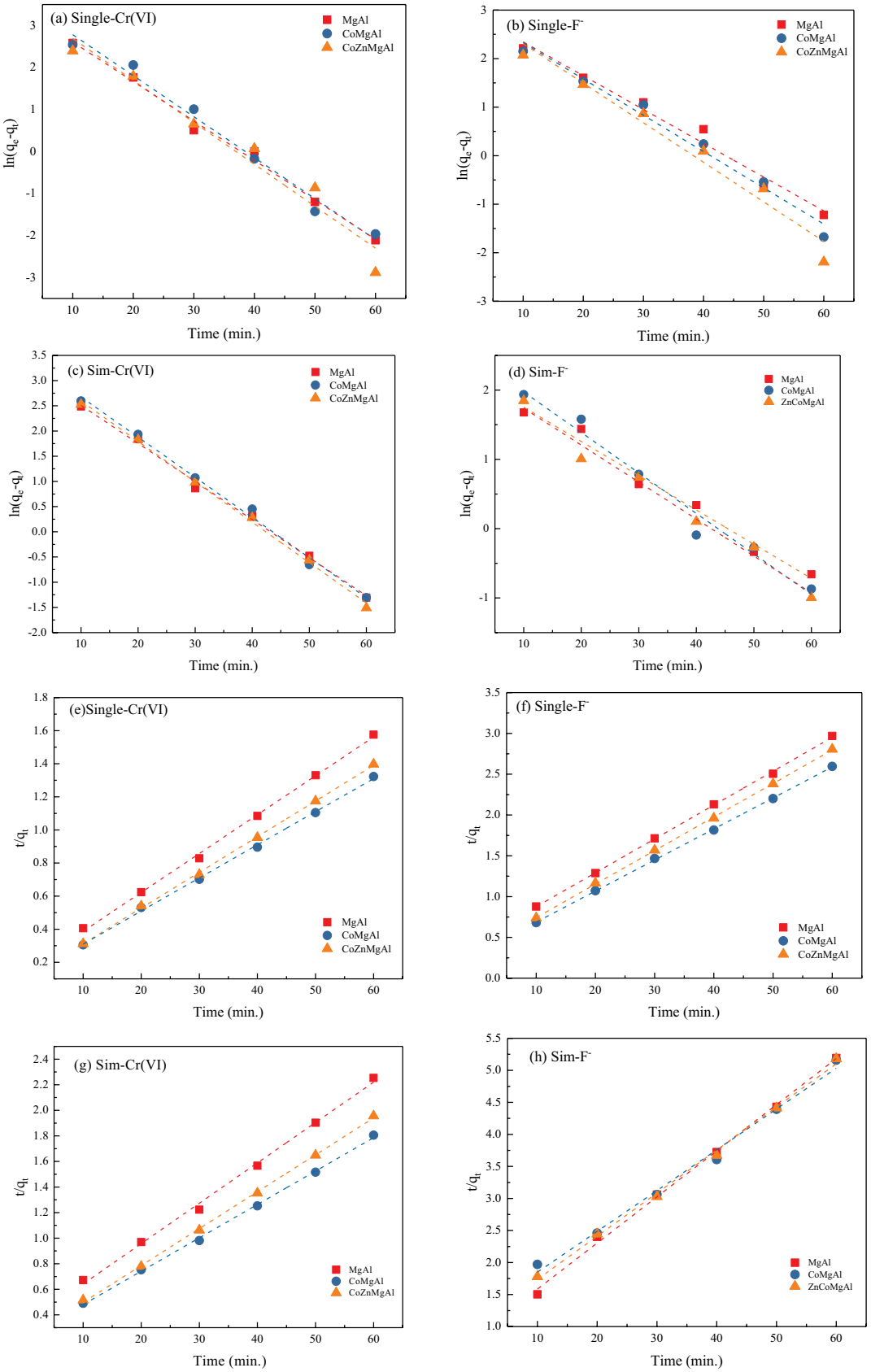

Fig. 7. (a), (b), (c) and (d) pseudo-first order, (e), (f), (g) and (h) pseudo-second order for the single/simultaneous adsorption of Cr(VI) and fluoride using LDHs ($V_{solution}$ = 250 mL, C_0 = 10 mg/L, dosage = 0.7 g/L, T = 298 K, initial pH about 7).

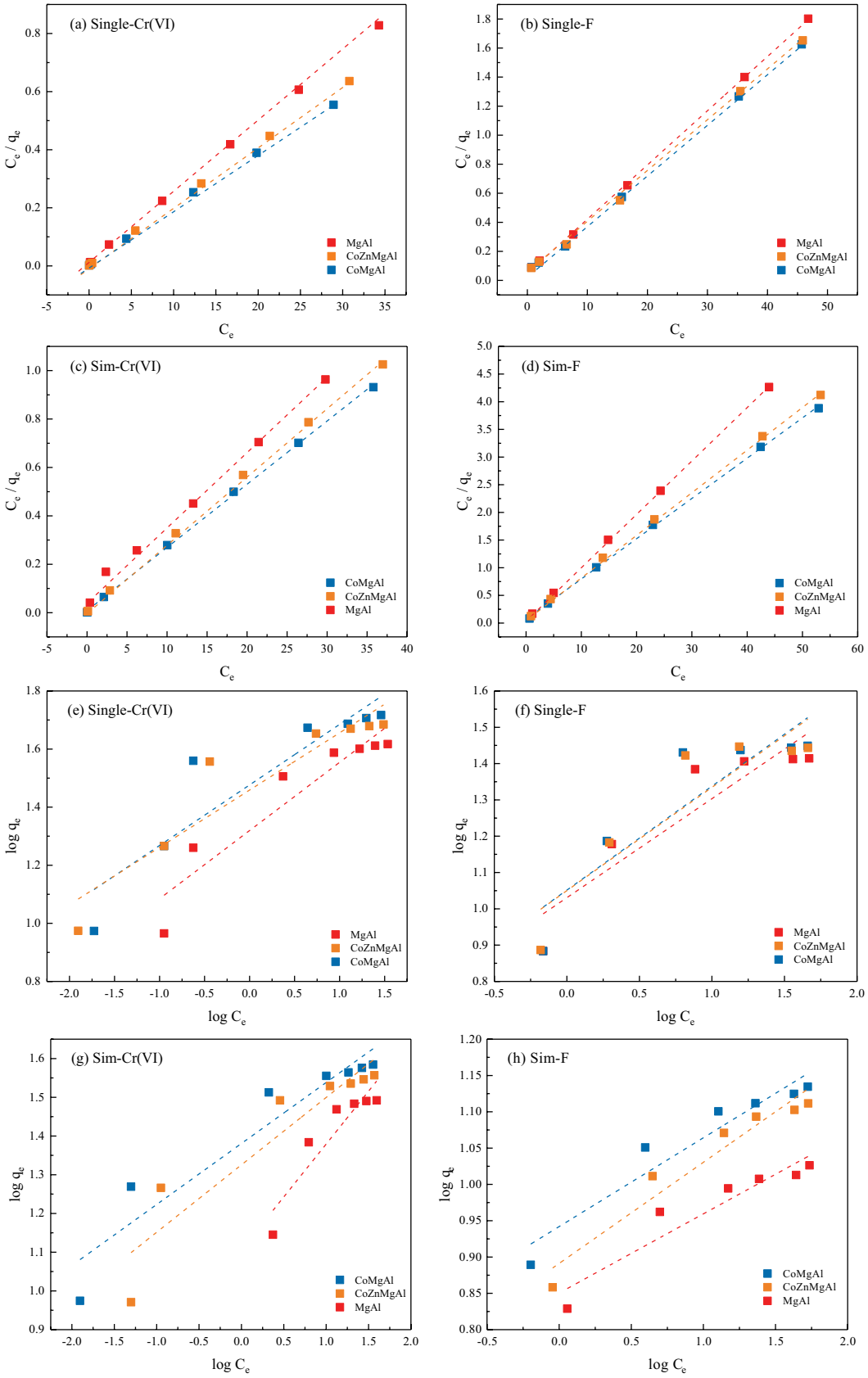

Fig. 8. (a), (b), (c) and (d) Langmuir, (e), (f), (g) and (h) Freundlich isotherm models for the single/simultaneous adsorption of Cr(VI) and fluoride using LDHs ($V_{solution}$ = 250 mL, C_0 = 10 mg/L, dosage = 0.7 g/L, T = 298 K, initial pH about 7).

Adsorption isotherms are important for the adsorption process and they are used to determine the adsorption capacities of adsorbents and the type of adsorption taking place [40]. Linear Langmuir and Freundlich isotherm models were employed to analyze the experimental data in Fig. 8.

The equations are represented as follows [41]:

Langmuir isotherm:

$$\frac{C_e}{q_e} = \frac{1}{K_L Q_m} + \frac{C_e}{Q_m} \tag{5}$$

The linear regression between C_e/q_e vs. C_e allows the computation of R^2 value, which conforms to be 0.99, referring the monolayer adsorption of Cr(VI) and fluoride onto LDHs. In simultaneous adsorption, it could be observed that the removal capacity of all LDHs was weakened, but the fluoride removal capacity decreased significantly. CoMgAl-LDH removed more Cr(VI) and fluoride than MgAl-LDH and CoZnMgAl-LDH in the same time interval, and the maximum adsorption capacity of Cr(VI) and fluoride reached 52.63 and 29.41 mg/g, respectively (Table 2).

Another essential component of Langmuir isotherm can be denoted in terms of a dimensionless constant called separation factor R_L determined as follows:

$$R_L = \frac{1}{1 + K_L C_0} \tag{6}$$

where C_0 (mg/L) is the lowest initial Cr(VI) or fluoride concentration and b is Langmuir constant (L/mg). The value of R_L indicates the type of the isotherm to be either unfavorable ($R_L > 1$), linear ($R_L = 1$), favorable ($0 < R_L < 1$) or irreversible ($R_L = 0$). In the present study, the values of R_L were <1, which indicated favorable adsorption during the whole range of Cr(VI) and fluoride concentration in single and simultaneous adsorption [30].

Freundlich isotherm:

$$\log q_e = \log k_f + \frac{1}{n} \log C_e \tag{7}$$

where k_f and n are the Freundlich adsorption constants which were determined from the intercept and slope of the linear plots of $\log q_e$ vs. $\log C_e$, respectively.

The Langmuir and Freundlich parameters are listed in Table 2. The higher values of correlation coefficients ($R^2 > 0.997$) for Langmuir model than that of Freundlich model suggested monolayer rather than multilayer adsorption occurred onto LDHs. Due to the lower value of correlation coefficient for the Freundlich isotherm model, this model could not properly describe the relationship between the amounts of adsorbed Cr(VI) and fluoride ions and their equilibrium concentrations in the solutions. In view of excellent adsorption performance, CoMgAl-LDH was selected for further analysis of pollutant adsorption mechanism. In addition, a comparison of maximum monolayer adsorption capacity of Cr(VI) or fluoride onto various adsorbents is shown in Table 3. By contrast, CoMgAl-LDH possessed higher maximum monolayer adsorption capacity of Cr(VI) or fluoride than most adsorbents shown in Table 2.

3.2.5. Adsorption mechanism by the CoMgAl-LDH

The particle morphology and chemical composition of the CoMgAl-LDH before and after adsorption of fluoride and Cr(VI) can be seen in the SEM images and corresponding EDX spectrum presented in Fig. 9. The SEM image of CoMgAl-LDH showed a distinct layered structure, and no structural changes were observed after adsorption of Cr(VI) and fluoride. Corresponding EDX spectrum showed the presence of Mg, O, Al, Co, Cl, indicating CoMgAl-LDH was successfully prepared and the presence of fluoride and Cr(VI) in CoMgAl-LDH after adsorption of fluoride and Cr(VI), verifying the adsorption of fluoride and Cr(VI) by CoMgAl-LDH.

Table 2
Adsorption isotherm constants parameters for the single/simultaneous adsorption of Cr(VI) and fluoride on the LDHs with dosage at 0.7 g/L

Item		Langmuir constants				Freundlich constants		
		Q_m (mg/g)	b (L/mg)	R_L	R^2	$1/n$	K_F	R^2
Single-Cr(VI)	MgAl-LDH	41.67	0.011	0.95	0.997	0.235	20.87	0.886
	CoMgAl-LDH	52.63	0.005	0.98	0.998	0.198	30.81	0.840
	CoZnMgAl-LDH	48.45	0.005	0.98	0.999	0.197	28.76	0.878
Single-F^-	MgAl-LDH	26.79	0.048	0.81	0.999	0.273	10.732	0.843
	CoMgAl-LDH	29.41	0.045	0.82	0.997	0.286	11.26	0.808
	CoZnMgAl-LDH	28.57	0.042	0.83	0.998	0.284	11.22	0.817
Simultaneous-Cr(VI)	MgAl-LDH	32.82	0.059	0.77	0.997	0.292	12.10	0.949
	CoMgAl-LDH	38.30	0.008	0.96	0.999	0.158	24.03	0.907
	CoZnMgAl-LDH	35.93	0.011	0.95	0.998	0.174	21.16	0.867
Simultaneous-F^-	MgAl-LDH	10.68	0.091	0.69	0.999	0.109	7.087	0.871
	CoMgAl-LDH	13.74	0.068	0.75	0.999	0.122	8.749	0.904
	CoZnMgAl-LDH	13.12	0.092	0.68	0.999	0.139	7.784	0.924

Table 3
List of various adsorbents (with maximum adsorption capacities) for the adsorption of Cr(VI) and fluoride

Adsorbate type	Adsorbents	Maximum adsorption capacity (mg/g)	Refs.
Cr(VI)	Green alga (raw and modified)	35	[42]
	Active carbon	7.2	[43]
	Carbon slurry	15.2	[44]
	CoMgAl-LDH	52.63	Present study
	Activated clay	24.1	[45]
	Treated rectorite	21	[46]
Fluoride	Modified Na–attapulgite	24.6	[47]
	Red mud	8.92	[48]
	Active carbon	2.7	[49]
	Activated quartz	1.6	[50]
	Quick lime	16.7	[51]
	CoMgAl-LDH	29.41	Present study

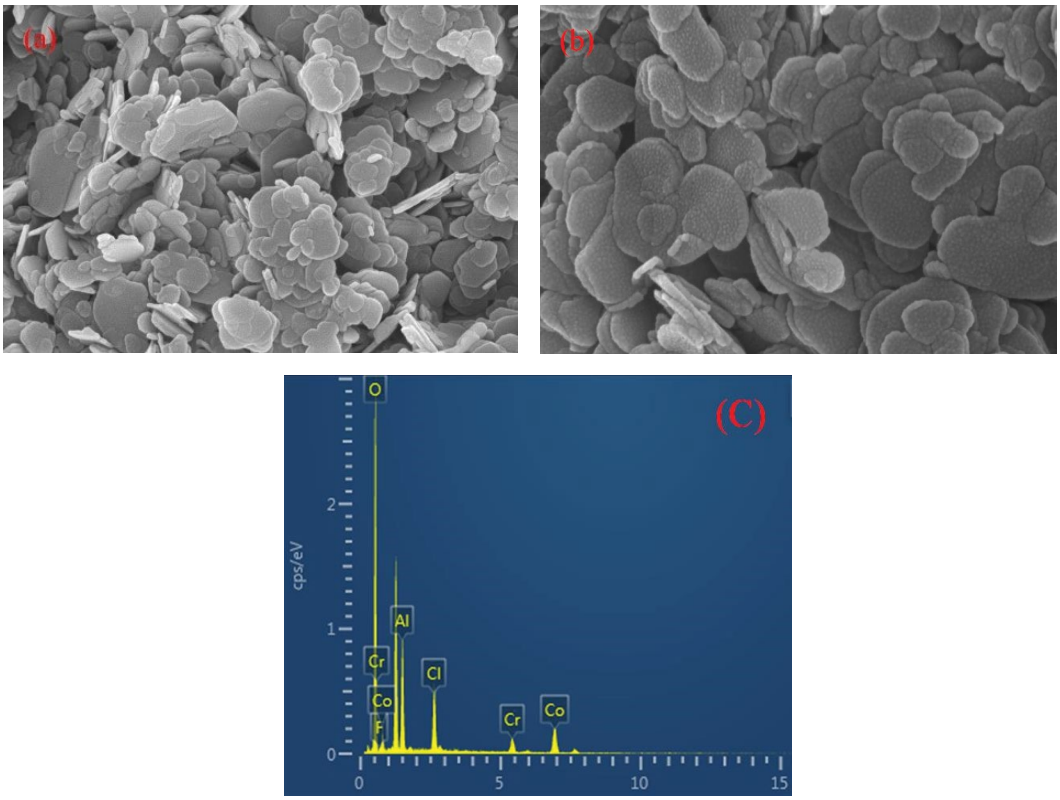

Fig. 9. SEM images and corresponding EDX spectrum of (a) CoMgAl-LDH before adsorption, (b) CoMgAl-LDH after adsorption of Cr(VI) and fluoride and (c) CoMgAl-LDH after adsorption of Cr(VI) and fluoride.

LDHs adsorbed anions benefitting from their anion exchange properties mainly. There existed weak electrostatic interaction with layers, and hence these anions could be easily replaced by the anions with higher electrostatic interaction with layers [52]. Cr(VI) and fluoride were intercalated into the interlayer of the CoMgAl-LDH spontaneously by anion exchange because Cr(VI) and fluoride had stronger electrostatic interaction than chloride ions for LDHs materials. The XRD patterns of CoMgAl-LDH before and after Cr(VI), fluoride and Cr(VI) + fluoride removal are shown in Fig. 10a.

Similar with other reports, the samples showed a similar structure to the original LDHs, and no extra peak was observed [21,53]. However, some slight variations of the basic parameter of LDHs were occurred. In Table 4, the value of basal spacing in connection with radius of interlayer anions increased from 0.792 to 0.799 nm after single Cr(VI)

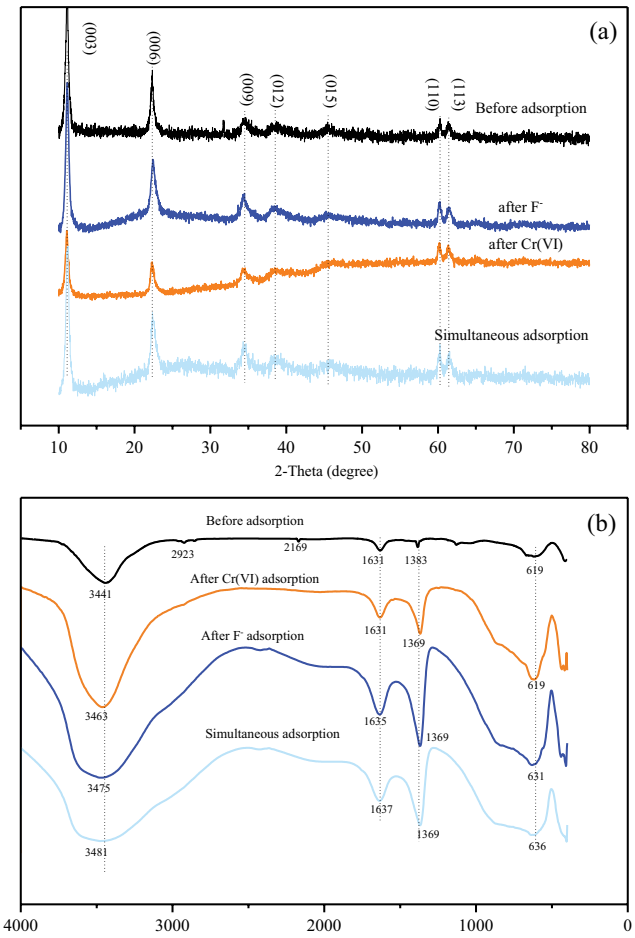

Fig. 10. (a) XRD patterns and (b) FTIR spectra of CoMgAl-LDH before and after Cr(VI) and F^- adsorption at C_0 = 10 mg/L with dosage of 0.7 g/L, 298 K, initial pH about 7.

Table 4
General characteristics of the CoMgAl-LDH before and after adsorption

Samples	Basal spacing (nm)	*a* (nm)	*c* (nm)
Before	0.792	0.306	2.376
S-Cr	0.799	0.306	2.397
S-F	0.788	0.306	2.364
Simultaneous	0.794	0.306	2.382

Lattice parameters *a* and *c* are obtained via equation: $a = 2d_{110}$ and $c = 3d_{003}$, respectively.

adsorption, and reduced to 0.788 nm after single fluoride adsorption. Basal spacing was neutralized to 0.794 nm after Cr(VI) + fluoride adsorption. The results were in accordance with the ion radius order: Cr(VI) > Cl^- > F^- and supported the removal mechanism of ion exchange that occurred in the interlayer of the LDHs.

Further evidence to explain that ion exchange occurred during adsorption process could be obtained by FTIR spectra, which is shown in Fig. 10b. Four major peaks including peak I (~3,450 cm^{-1}, hydroxyl groups stretching), peak

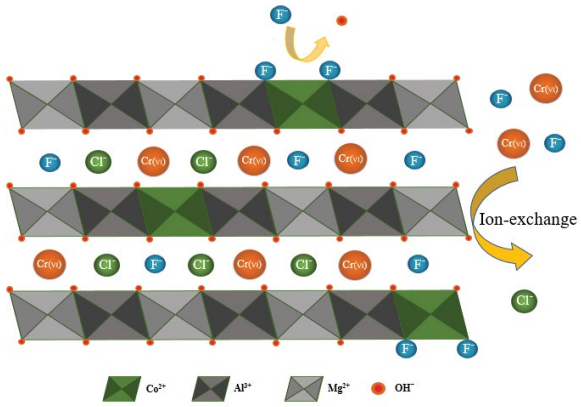

Fig. 11. Possible adsorption mechanisms.

II (~1,631 cm^{-1}, C=O), peak III (~1,383 cm^{-1}, C–O stretching of CO^{3-} ions), and peak IV (~619cm^{-1}, metal–O stretching) appeared on all samples before and after adsorption [54]. Peak I changed from 3,441 to 3,463/3,475 cm^{-1} after single Cr(VI) or fluoride adsorption. Furthermore, it expanded to 3,481 cm^{-1} after simultaneous adsorption of Cr(VI) and fluoride, indicating that compared with the single adsorption more numerous hydroxyl groups existing in the interlayer or surface of the CoMgAl-LDH participated in the simultaneous adsorption process [35]. After adsorption, peak at 2,169 cm^{-1} disappeared and peak III shifted to 1,369 cm^{-1} indicating that ion exchange occurred between Cr(VI)/F^- and CO^{3-} ions. The results could be attributed to the strong electrostatic forces between Cr(VI)/F^- and CoMgAl-LDH lattice. Comparing with the intact peak IV (619 cm^{-1}) after Cr(VI) adsorption, peak IV shifted to higher wavenumber (631/636 cm^{-1}) after single/simultaneous fluoride adsorption, suggesting that the bond of M–O changed in the adsorption process as follows: M–OH + F^- → M–F + OH^- (around natural pH), where M stands for Co, Mg and Al [55]. Through the previous analysis, the possible adsorption mechanisms are summarized in Fig. 11. Ion exchange was the mutual way to remove Cr(VI) and fluoride in the LDHs. This result further confirmed the report on the adsorption mechanism of Cr(VI) and fluoride [13,56].

4. Conclusion

Three types of multiple metal LDHs were synthesized and used in single/simultaneous adsorption of Cr(VI) and fluoride from aqueous solution. CoMgAl-LDH expressed the best structure and pollutant removal performance among the three LDHs. Introduction of Co enhanced the adsorption performance for Cr(VI) and fluoride. In the single adsorption, the CoMgAl-LDH showed excellent adsorption capacity of 52.63 mg/g for Cr(VI) and 29.41 mg/g for fluoride. Adsorption of Cr(VI) and fluoride on the LDHs was consistent with the pseudo-second order model and the equilibrium data fitted well with Langmuir isotherm both in the single adsorption system and simultaneous system. In simultaneous adsorption, Cr(VI) and fluoride competed for adsorption sites on the LDHs, and the results showed that fluoride suffered a more severe influence than Cr(VI).

The curve fits of data and mechanism analysis indicated that interlayer ion exchange was the main adsorption path for Cr(VI) and fluoride removal. Due to the low cost, easy preparation and high adsorption capacity, CoMgAl-LDH was a potentially developed adsorbent for simultaneous removal of Cr(VI) and fluoride from groundwater.

Acknowledgment

This research was supported by the International Scientific and Technological Innovation and Cooperation Project of Sichuan (No. 2019YFH0170).

References

[1] X. Bai, Y. Du, X. Hu, Y. He, C. He, E. Liu, J. Fan, Synergy removal of Cr (VI) and organic pollutants over RP-MoS_2/rGO photocatalyst, Appl. Catal., B, 239 (2018) 204–213.
[2] M.S. Gaikwad, C. Balomajumder, Simultaneous electrosorptive removal of chromium(VI) and fluoride ions by capacitive deionization (CDI): multicomponent isotherm modeling and kinetic study, Sep. Purif. Technol., 186 (2017) 272–281.
[3] S. Ayoob, A.K. Gupta, Fluoride in drinking water: a review on the status and stress effects, Crit. Rev. Environ. Sci. Technol., 36 (2006) 433–487.
[4] L. Deng, Z. Shi, L. Wang, S. Zhou, Fabrication of a novel $NiFe_2O_4$/Zn-Al layered double hydroxide intercalated with EDTA composite and its adsorption behavior for Cr(VI) from aqueous solution, J. Phys. Chem. Solids, 104 (2017) 79–90.
[5] Z.A. Al-Othman, R. Ali, M. Naushad, Hexavalent chromium removal from aqueous medium by activated carbon prepared from peanut shell: adsorption kinetics, equilibrium and thermodynamic studies, Chem. Eng. J., 184 (2012) 238–247.
[6] G. Sharma, A. Kumar, M. Naushad, A. Kumar, A.a.H. Al-Muhtaseb, P. Dhiman, A.A. Ghfar, F.J. Stadler, M.R. Khan, Photoremediation of toxic dye from aqueous environment using monometallic and bimetallic quantum dots based nanocomposites, J. Cleaner Prod., 172 (2018) 2919–2930.
[7] G. Sharma, B. Thakur, M. Naushad, A.a.H. Al-Muhtaseb, A. Kumar, M. Sillanpaa, G.T. Mola, Fabrication and characterization of sodium dodecyl sulphate@ironsilicophosphate nanocomposite: ion exchange properties and selectivity for binary metal ions, Mater. Chem. Phys., 193 (2017) 129–139.
[8] Y. Zheng, B. Cheng, W. You, J. Yu, W. Ho, 3D hierarchical graphene oxide-NiFe LDH composite with enhanced adsorption affinity to Congo red, methyl orange and Cr(VI) ions, J. Hazard. Mater., 369 (2019) 214–225.
[9] M. Naushad, T. Ahamad, G. Sharma, A.a.H. Al-Muhtaseb, A.B. Albadarin, M.M. Alam, Z.A. Alothman, S.M. Alshehri, A.A. Ghfar, Synthesis and characterization of a new starch/SnO_2 nanocomposite for efficient adsorption of toxic Hg^{2+} metal ion, Chem. Eng. J., 300 (2016) 306–316.
[10] G. Sharma, B. Thakur, M. Naushad, A. Kumar, F.J. Stadler, S.M. Alfadul, G.T. Mola, Applications of nanocomposite hydrogels for biomedical engineering and environmental protection, Environ. Chem. Lett., 16 (2017) 113–146.
[11] G. Sharma, M. Naushad, D. Pathania, A. Mittal, G.E. El-desoky, Modification of *Hibiscus cannabinus* fiber by graft copolymerization: application for dye removal, Desal. Wat. Treat., 54 (2014) 3114–3121.
[12] M.A. Teixeira, A.B. Mageste, A. Dias, L.S. Virtuoso, K.P.F. Siqueira, Layered double hydroxides for remediation of industrial wastewater containing manganese and fluoride, J. Cleaner Prod., 171 (2018) 275–284.
[13] H.P. Chao, Y.C. Wang, H.N. Tran, Removal of hexavalent chromium from groundwater by Mg/Al-layered double hydroxides using characteristics of in-situ synthesis, Environ. Pollut., 243 (2018) 620–629.
[14] M. Xu, B. Bi, B. Xu, Z. Sun, L. Xu, Polyoxometalate-intercalated ZnAlFe-layered double hydroxides for adsorbing removal and photocatalytic degradation of cationic dye, Appl. Clay Sci., 157 (2018) 86–91.
[15] T.L. Coelho, Y.E. Licea, L.A. Palacio, A.C. Faro, Heptamolybdate-intercalated CoMgAl hydrotalcites as precursors for HDS-selective hydrotreating catalysts, Catal. Today, 250 (2015) 38–46.
[16] B. Zhang, L. Luan, R. Gao, F. Li, Y. Li, T. Wu, Rapid and effective removal of Cr(VI) from aqueous solution using exfoliated LDH nanosheets, Colloids Surf., A, 520 (2017) 399–408.
[17] D. Bharali, R.C. Deka, Preferential adsorption of various anionic and cationic dyes from aqueous solution over ternary CuMgAl layered double hydroxide, Colloids Surf., A, 525 (2017) 64–76.
[18] S. Anantharaj, K. Karthick, S. Kundu, Evolution of layered double hydroxides (LDH) as high performance water oxidation electrocatalysts: a review with insights on structure, activity and mechanism, Mater. Today Energy, 6 (2017) 1–26.
[19] M. Pigna, J.J. Dynes, A. Violante, A. Sommella, A.G. Caporale, Sorption of arsenite on Cu-Al, Mg-Al, Mg-Fe, and Zn-Al layered double hydroxides in the presence of inorganic anions commonly found in aquatic environments, Environ. Eng. Sci., 33 (2016) 98–104.
[20] J. Cai, X. Zhao, Y. Zhang, Q. Zhang, B. Pan, Enhanced fluoride removal by La-doped Li/Al layered double hydroxides, J. Colloid Interface Sci., 509 (2018) 353–359.
[21] X. He, X. Qiu, J. Chen, Preparation of Fe(II)–Al layered double hydroxides: application to the adsorption/reduction of chromium, Colloids Surf. A, 516 (2017) 362–374.
[22] P. Cai, H. Zheng, C. Wang, H. Ma, J. Hu, Y. Pu, P. Liang, Competitive adsorption characteristics of fluoride and phosphate on calcined Mg-Al-CO_3 layered double hydroxides, J. Hazard. Mater., 213–214 (2012) 100–108.
[23] A. Nagaraj, M. Rajan, Enhanced removal of hazardous fluoride from drinking water by using a smart material: magnetic iron oxide fabricated layered double hydroxide/cellulose composite, J. Environ. Chem. Eng., 6 (2018) 5645–5654.
[24] A.A. Bakr, N.A. Sayed, T.M. Salama, I.O. Ali, R.R. Abdel Gayed, N.A. Negm, Kinetics and thermodynamics of Mn(II) removal from aqueous solutions onto Mg-Zn-Al LDH/montmorillonite nanocomposite, Egypt. J. Petrol., 27 (2018) 1215–1220.
[25] F. Ling, L. Fang, Y. Lu, J. Gao, F. Wu, M. Zhou, B. Hu, A novel CoFe layered double hydroxides adsorbent: High adsorption amount for methyl orange dye and fast removal of Cr(VI), Microporous Mesoporous Mater., 234 (2016) 230–238.
[26] X. Tao, D. Liu, W. Cong, L. Huang, Controllable synthesis of starch-modified ZnMgAl-LDHs for adsorption property improvement, Appl. Surface Sci., 457 (2018) 572–579.
[27] W. Wang, J. Zhou, G. Achari, J. Yu, W. Cai, Cr(VI) removal from aqueous solutions by hydrothermal synthetic layered double hydroxides: adsorption performance, coexisting anions and regeneration studies, Colloids Surf., A, 457 (2014) 33–40.
[28] A. Jawad, Y. Li, X. Lu, Z. Chen, W. Liu, G. Yin, Controlled leaching with prolonged activity for Co-LDH supported catalyst during treatment of organic dyes using bicarbonate activation of hydrogen peroxide, J. Hazard. Mater., 289 (2015) 165–173.
[29] F. Yang, S. Zhang, Y. Sun, K. Cheng, J. Li, D.C.W. Tsang, Fabrication and characterization of hydrophilic corn stalk biochar-supported nanoscale zero-valent iron composites for efficient metal removal, Bioresour. Technol., 265 (2018) 490–497.
[30] H. Hu, J. Liu, Z. Xu, L. Zhang, B. Cheng, W. Ho, Hierarchical porous Ni/Co-LDH hollow dodecahedron with excellent adsorption property for Congo red and Cr(VI) ions, Appl. Surface Sci., 478 (2019) 981–990.
[31] L. Hongtao, L. Shuxia, Z. Hua, Q. Yanling, Y. Daqiang, Z. Jianfu, Z. Zhiliang, Comparative study on synchronous adsorption of arsenate and fluoride in aqueous solution onto MgAlFe-LDHs with different intercalating anions, RSC Adv., 8 (2018) 33301–33313.
[32] M. Islam, R. Patel, Synthesis and physicochemical characterization of Zn/Al chloride layered double hydroxide and evaluation of its nitrate removal efficiency, Desalination, 256 (2010) 120–128.
[33] S. Yanming, L. Dongbin, L. Shifeng, F. Lihui, C. Shuai, M.A. Haque, Removal of lead from aqueous solution on glutamate

intercalated layered double hydroxide, Arab. J. Chem., 10 (2017) S2295–S2301.
[34] X. Lv, X. Qin, K. Wang, Y. Peng, P. Wang, G. Jiang, Nanoscale zero valent iron supported on MgAl-LDH-decorated reduced graphene oxide: enhanced performance in Cr(VI) removal, mechanism and regeneration, J. Hazard. Mater., 373 (2019) 176–186.
[35] J. Wang, D. Kang, X. Yu, M. Ge, Y. Chen, Synthesis and characterization of Mg–Fe–La trimetal composite as an adsorbent for fluoride removal, Chem. Eng. J., 264 (2015) 506–513.
[36] X. Wu, Y. Zhang, X. Dou, M. Yang, Fluoride removal performance of a novel Fe–Al–Ce trimetal oxide adsorbent, Chemosphere, 69 (2007) 1758–1764.
[37] K.H. Goh, T.T. Lim, Z. Dong, Application of layered double hydroxides for removal of oxyanions: a review, Water Res., 42 (2008) 1343–1368.
[38] R.L. Goswamee, P. Sengupta, K.G. Bhattacharyya, D.K. Dutta, Adsorption of Cr(VI) in layered double hydroxides, Appl. Clay Sci., 13 (1998) 21–34.
[39] M. Naushad, S. Vasudevan, G. Sharma, A. Kumar, Z.A. Alothman, Adsorption kinetics, isotherms, and thermodynamic studies for Hg^{2+} adsorption from aqueous medium using alizarin red-S-loaded amberlite IRA-400 resin, Desal. Wat. Treat., 57 (2015) 18551–18559.
[40] G. Sharma, M. Naushad, A.a.H. Al-Muhtaseb, A. Kumar, M.R. Khan, S. Kalia, Shweta, M. Bala, A. Sharma, Fabrication and characterization of chitosan-crosslinked-poly(alginic acid) nanohydrogel for adsorptive removal of Cr(VI) metal ion from aqueous medium, Int. J. Biol. Macromol., 95 (2017) 484–493.
[41] G. Sharma, M. Naushad, A. Kumar, S. Rana, S. Sharma, A. Bhatnagar, F.J. Stadler, A.A. Ghfar, M.R. Khan, Efficient removal of coomassie brilliant blue R-250 dye using starch/poly(alginic acid-cl-acrylamide) nanohydrogel, Process Saf. Environ. Protect., 109 (2017) 301–310.
[42] V.K. Gupta, A.K. Shrivastava, N. Jain, Biosorption of chromium(VI) from aqueous solutions by green algae Spirogyra species, Water Res., 35 (2001) 4079–4085.
[43] F.D. Natale, A. Erto, A. Lancia, D. Musmarra, A descriptive model for metallic ions adsorption from aqueous solutions onto activated carbons, J. Hazard. Mater., 169 (2009) 360–369.
[44] V.K. Gupta, A. Rastogi, A. Nayak, Adsorption studies on the removal of hexavalent chromium from aqueous solution using a low cost fertilizer industry waste material, J. Colloid Interface Sci., 342 (2010) 135–141.
[45] W. Li, Y. Tang, Y. Zeng, Z. Tong, D. Liang, W. Cui, Adsorption behavior of Cr(VI) ions on tannin-immobilized activated clay, Chem. Eng. J., 193–194 (2012) 88–95.
[46] H. Hong, W.T. Jiang, X. Zhang, L. Tie, Z. Li, Adsorption of Cr(VI) on STAC-modified rectorite, Appl. Clay Sci., 42 (2008) 292–299.
[47] G. Zhang, Z. He, X. Wei, A low-cost and high efficient zirconium-modified-Na-attapulgite adsorbent for fluoride removal from aqueous solutions, Chem. Eng. J., 183 (2012) 315–324.
[48] A. Tor, N. Danaoglu, G. Arslan, Y. Cengeloglu, Removal of fluoride from water by using granular red mud: Batch and column studies, J. Hazard. Mater., 164 (2009) 271–278.
[49] M.S. Gaikwad, C. Balomajumder, Tea waste biomass activated carbon electrode for simultaneous removal of Cr(VI) and fluoride by capacitive deionization, Chemosphere, 184 (2017) 1141–1149.
[50] X. Fan, D.J. Parker, M.D. Smith, Adsorption kinetics of fluoride on low cost materials, Water Res., 37 (2003) 4929–4937.
[51] M. Islam, R.K. Patel, Evaluation of removal efficiency of fluoride from aqueous solution using quick lime, J. Hazard. Mater., 43 (2007) 303–310.
[52] G. Mishra, B. Dash, S. Pandey, Layered double hydroxides: A brief review from fundamentals to application as evolving biomaterials, Appl. Clay Sci., 153 (2018) 172–186.
[53] V. Hernandez-Montoya, M.A. Perez-Cruz, D.I. Mendoza-Castillo, M.R. Moreno-Virgen, A. Bonilla-Petriciolet, Competitive adsorption of dyes and heavy metals on zeolitic structures, J. Environ. Manage., 116 (2013) 213–221.
[54] S. Chen, Y. Huang, X. Han, Z. Wu, C. Lai, J. Wang, Q. Deng, Z. Zeng, S. Deng, Simultaneous and efficient removal of Cr(VI) and methyl orange on LDHs decorated porous carbons, Chem. Eng. J., 352 (2018) 306–315.
[55] T. Zhang, Q. Li, H. Xiao, H. Lu, Y. Zhou, Synthesis of Li–Al layered double hydroxides (LDHs) for efficient fluoride removal, Ind. Eng. Chem. Res., 51 (2012) 11490–11498.
[56] P. Huang, C. Cao, F. Wei, Y.B. Sun, W. Song, MgAl layered double hydroxides with chloride and carbonate ions as interlayer anions for removal of arsenic and fluoride ions in water, RSC Adv., 5 (2015) 10412–10417.